Fluorescence Microscopy Evidence for Quasi-Permanent Attachment of Antifreeze Proteins to Ice Surfaces

Natalya Pertaya,* Christopher B. Marshall,† Carlos L. DiPrinzio,* Larry Wilen,* Erik S. Thomson,‡ J. S. Wettlaufer,‡§ Peter L. Davies,† and Ido Braslavsky*

*Department of Physics and Astronomy, Ohio University, Athens, Ohio; †Department of Biochemistry, Queen's University, Kingston, Ontario, Canada; and ‡Department of Geology and Geophysics, §Department of Physics, Yale University, New Haven, Connecticut

ABSTRACT Many organisms are protected from freezing by the presence of extracellular antifreeze proteins (AFPs), which bind to ice, modify its morphology, and prevent its further growth. These proteins have a wide range of applications including cryopreservation, frost protection, and as models in biomineralization research. However, understanding their mechanism of action remains an outstanding challenge. While the prevailing adsorption-inhibition hypothesis argues that AFPs must bind irreversibly to ice to arrest its growth, other theories suggest that there is exchange between the bound surface proteins and the free proteins in solution. By conjugating green fluorescence protein (GFP) to a fish AFP (Type III), we observed the binding of the AFP to ice. This was accomplished by monitoring the presence of GFP-AFP on the surface of ice crystals several microns in diameter using fluorescence microscopy. The lack of recovery of fluorescence after photobleaching of the GFP component of the surface-bound GFP-AFP shows that there is no equilibrium surface-solution exchange of GFP-AFP and thus supports the adsorption-inhibition mechanism for this type of AFP. Moreover, our study establishes the utility of fluorescently labeled AFPs as a research tool for investigating the mechanisms underlying the activity of this diverse group of proteins.

INTRODUCTION

Antifreeze proteins (AFPs) protect animals from freezing by binding to extracellular ice and inhibiting its growth (1–3). They were first found some 35 years ago in certain fish that can survive in seawater that is colder than the typical freezing temperature of fish blood (4). Since then, AFPs have also been found in arthropods (5,6), plants (7,8), bacteria (9,10), and fungi (11). AFPs are interesting because of the fundamental challenges associated with understanding their antifreeze activity, and also provide promising approaches to the protection of other fish, crops, and tissues (12–17).

AFPs are usually grouped according to their structures. There are five known types of fish AFPs (18); for example, Type I AFPs have a 3–4 kDa α-helix structure (19), whereas Type III AFPs are 6.5 kDa β-clip globular proteins. AFPs from other organisms have other structures, such as the β-helical spruce budworm AFP (20). These different structures have affinities to different ice planes, and hence give rise to different ice crystal shapes. The activity of an AFP is usually characterized by measuring its thermal hysteresis, i.e., the extent to which the nonequilibrium freezing point of ice is reduced below the melting point. The thermal hysteresis of AFPs varies as a function of concentration, and the specific activity of different AFP types ranges over two orders of magnitude from hyperactive to moderate to weak (21).

The generally accepted ''adsorption-inhibition'' (1,22–24) mechanism for AFP activity proposes that the specific binding of these proteins to an ice surface results in the inhibition of ice growth because of the Kelvin effect (22). The binding of the protein to the surface is principally due to the entropic effects of docking the relatively hydrophobic flat protein surface to ice, and to the formation of a few hydrogen bonds (1,25–28). The ice surface is pinned by the adsorbed AFPs and the accumulation of bound proteins is limited by the curvature of their microsurfaces (23,29). As a result, the nonequilibrium freezing point is lowered below the melting point, and within this thermal hysteresis gap, the ice crystals appear by light microscopy to be stable, neither growing nor melting (30). Such ice crystals usually have a characteristic faceted morphology that results from the inhibition of the growth of the crystal surfaces to which the AFP binds. This has been most convincingly demonstrated for the Type I AFP from winter flounder, for which both the binding plane and the direction of binding have been determined using a technique called ice etching (31). The binding plane defines a hexagonal bipyramidal crystal with a predicted c/a axial ratio of 3.3:1, a result that is consistently obtained for this AFP (32). Other fish AFPs, such as the Type III AFP from ocean pout, produce hexagonal bipyramidal crystals with a more variable morphology. The crystal axial ratio in the presence of Type III AFP is affected both by dilution and by mutation of surface residues, possibly because this type of AFP can bind to more than one ice plane (32, 33).

It has been argued that AFPs have to bind irreversibly to prevent ice growth, because in the presence of a 10^4–10^7-fold molar excess of water even transient desorption of AFPs would allow water molecules to join the ice lattice at the newly exposed sites. Thus, without irreversible binding the crystal would keep growing, albeit at a decreased rate (34).

Submitted September 1, 2006, and accepted for publication January 25, 2007.

Address reprint requests to Ido Braslavsky, Tel.: 740-597-3011; E-mail: braslavs@ohiou.edu.

0006-3495/07/05/3663/11 $2.00

doi: 10.1529/biophysj.106.096297

This conclusion has been criticized (35,36) on the grounds that the dependence of the thermal hysteresis on concentration suggests there is some form of equilibrium exchange of bound and unbound proteins (37,38). The calculated free energy of bound proteins is only a few kT lower than that of unbound proteins (39). The suggestion that the water/ice boundary is not sharp, i.e., that there is a quasi-liquid at the water/ice interface, has raised doubts about the idea that the AFP molecules are tightly bound to the surface (40,41). An alternative mechanism for the complete inhibition of crystal growth by AFP molecules is that their presence modifies the interfacial energy, a process that does not require irreversible attachment (35,41). Experimental adsorption kinetics evidence is sparse and does not exist at all for most AFPs. For Type I AFPs, it has been claimed that fast exchange of proteins occurs (42). Thus, we consider the irreversibility of AFP binding to ice to be an open question that requires further investigation and experimental validation.

It has been proposed (24,29) that, within the framework of adsorption-inhibition theory, the concentration dependence of thermal hysteresis activity might be explained by the interplay between the engulfment of the bound proteins by the ice, which would result in local ice growth, and the rate of patching of such a breach by molecules from the solution, which is a function of AFP concentration. How often this happens is not clear, but it should result in nonzero interface growth. It has previously been found by optical observation of ice crystals in AFP solutions that no growth or melt is visible for periods as long as a few days (22). If the accuracy of these observations is approximately a micron, the limit on surface growth is ~100 nm/day. Here we demonstrate that the accuracy of this experimental limit can be improved significantly.

The adsorption-inhibition theory predicts that the surface concentration of AFPs should not be a function of AFP concentration, but only of the number of available binding sites, as the off-rate should be close to zero. On the other hand, partial coverage of the surface is thought to be sufficient to inhibit its growth. Thus, accumulation of AFPs on the surface is expected to continue after the formation of the crystal. Experimental evidence for such accumulation has been obtained for antifreeze glycoproteins using ellipsometry (43).

To study the adsorption of AFPs onto ice, and in particular to determine the extent of exchange of bound proteins with free proteins, we produced a recombinant fusion protein consisting of green fluorescence protein (GFP) (44) linked to the N-terminus of Type III AFP derived from ocean pout (Fig. 1). The activity of the AFP is not diminished by this modification, because the N-terminus is remote from the AFP's ice-binding site (45), and so the GFP domain is positioned in an orientation that does not interfere with ice binding. In fact, the activity of such fusion proteins is slightly enhanced by their increased size (46). The use of this recombinant protein enables us to make direct observations of AFPs bound to ice. Direct observation of protein adsorbed onto crystals using fluorescence microscopy has provided a useful tool for studying other systems, such as the adherence of macromolecules to calcium tartrate crystals (47), and of antibody molecules to a semiconductor material (48). Furthermore, by photobleaching the adsorbed GFP-AFPs, which annuls the fluorescence signal from the bound proteins (49), and monitoring the recovery of the fluorescence signal, we were able to investigate the extent to which unbound GFP-AFP proteins adsorb onto a stable ice surface that is already covered by AFPs. Such adsorption would indicate the exchange of bound proteins with free proteins in the solution, or the engulfment of the adsorbed proteins by the ice, followed by adsorption of free proteins onto newly created binding sites.

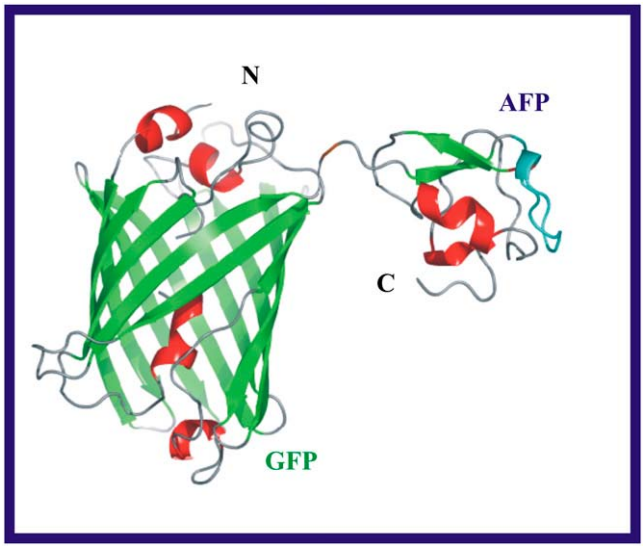

FIGURE 1 Ribbon diagram of the Type III antifreeze protein (AFP) linked through its N-terminus to the C-terminus of green fluorescence protein (GFP). The light blue region is the ice-binding site. The α-helices are shown in red and β-strands in green.

MATERIALS AND METHODS

Construction of the Type III GFP-AFP His-tagged fusion gene

The Type III AFP gene used for the fusion protein construct was a synthetic version of the ocean pout QAE-binding isoform (M1.1) in plasmid pT7-7F (46). The coding region was amplified by PCR using primers with a 5′-*Nde*I site and a 3′-*Xho*I site and no stop codon. The PCR product was cloned into the expression vector pET20b+ between its *Nde*I/*Xho*I sites in frame with the His tag sequence. Clones were screened by *Nde*I/*Xho*I digestion and sequencing. Vector containing the AFP insert was digested with *Nde*I, dephosphorylated with alkaline phosphatase and ligated with the GFP gene. The GFP gene segment was PCR amplified from pEGFP (Clontech, #6077-1, Mountain View, CA) using 5′ and 3′ primers each containing an *Nde*I restriction site. Additionally, the 3′ primer was designed to encode the linker sequence GlyAlaGly to separate the GFP from the Type III AFP. The GFP PCR product was gel-purified and digested with *Nde*I before ligation into the

Type III AFP pET20b His backbone. Resulting clones were screened for correct orientation by PCR using the T7 promoter and 3′ GFP primers, which produced an 800-basepair product only if the GFP insert was in the correct orientation. Clones that appeared to contain a correctly oriented insert were sequenced to confirm the presence of a gene encoding a full-length fusion product in the correct reading frame.

Expression and purification of the GFP-AFP protein

The GFP-AFP construct was expressed in *Escherichia coli* BL21(DE3) on a 1 L scale as previously described (46). The His-tagged fusion protein was purified from the cell lysate supernatant by Ni^{2+}-agarose affinity chromatography (7 mL, Qiagen, Valencia, CA) followed by ice affinity purification, which removes most solutes, including salts, contaminating proteins, GFP that is not attached to functional AFP, and misfolded AFP domains (50,51). The resulting ice fraction was concentrated using an Amicon ultracentrifugal filter device (Millipore, Billerica, MA) with a final yield of ~6 mg in 1 mL.

Experimental equipment

A thin cell consisting of two coverslips, 10 μm apart, sealed either with parafilm or with silicone elastomer (Sylgard 184, Dow Corning, Midland, MI) was used to hold the AFP and control solutions. This cell was placed in thermal contact with a custom-built temperature-controlled stage (Fig. 2). The stage includes a thermistor in conjunction with two thermoelectric cooling elements that are driven by a commercial temperature controller (Newport model 3150, Irvine, CA). Cold-water circulation was used as the heat sink for the thermoelectric cooling elements. Dry air was blown over the apparatus to keep it free of moisture. This arrangement permitted the cell temperature to be varied in the range from room temperature to −40°C with a precision of ±0.01°C. The time required for a 0.01°C change was 0.1 s. The samples were imaged using fluorescence microscopy. We used a confocal microscope (Zeiss LSM 510, Thornwood, NY), in the Ohio University confocal microscopy facility, equipped with a long working distance objective (Nikon Air 50× NA 0.55 ELWD 8.7 mm, Belmont, CA), and 488 nm and 633 nm laser illumination lines. The long-working-distance air objective enabled simple temperature control of the samples but did not enable acquisition of thin slices for three-dimensional imaging. Imaging 0.1 μm fluorescent beads (TetraSpeck microspheres, #T7279, Invitrogen, Carlsbad, CA) with the confocal microscope revealed that the point spread function (PSF) is approximately a three-dimensional Gaussian function (52) with an axial full-width at half-maximum of 4 ± 0.7 μm ($n = 10$) and a lateral full-width at half-maximum of 0.7 ± 0.08 μm ($n = 10$), in agreement with the expected PSF shape and size for this numerical aperture (53). However, with the use of this configuration we were able to significantly reduce the background compared to that present for wide-field fluorescence microscopy. The fluorescence signal was detected through a trichroic beam splitter (488/543/633 nm), a secondary dichroic beam splitter (545 nm), and two emission filters, a GFP filter (505–530 nm band pass) and a Cyanine-5 (Cy5) filter (650 nm high pass). We confirmed that there is negligible cross-talk of the GFP signal into the Cy5 filter and vice versa.

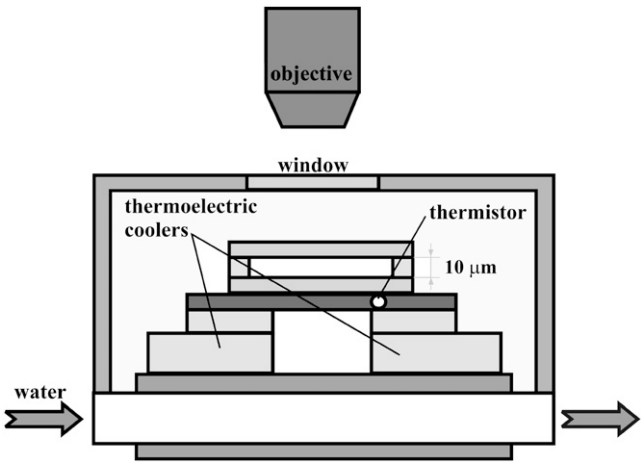

FIGURE 2 Experimental cell. A schematic drawing of the temperature-controlled cell. Details in text.

Signal analysis: evaluation of the signal from molecules bound to the ice surface

We used two approaches to measure the signal that originated from the surface. The first method used the signal from a free dye as a reference, whereas the second method used a bleached crystal as a reference point.

In the first method, the liquid contribution to the GFP-AFP signal was eliminated by subtracting it from the total signal. The liquid contribution was assumed to be proportional to the fluorescence intensity from Cy5, which is not conjugated to the AFP, in the GFP fluorescence image. This correction was carried out using the formula

$$I_{\text{subtraction1}} = (I_{\text{GFP}} - B_{\text{GFP}}) - C_1 \times (I_{\text{Cy5}} - B_{\text{Cy5}}), \qquad (1)$$

where C_1 is a constant set to null the background intensity in an area in which no crystal is present and is on the order of unity; I_{GFP} and I_{Cy5} are the intensities of the fluorescence produced with 488 nm and 633 nm illumination lines through the GFP filter and the Cy5 filter, respectively, measured in instrumental counts; and B_{GFP} and B_{Cy5} are the background levels, which were determined from measurements using the two filters for a sample that contained only buffer. We averaged the calculated intensity, $I_{\text{subtraction1}}$, over the peripheral ice region to obtain the contribution of GFP-AFPs bound to the ice crystal, $\bar{I}_{\text{subtraction1}}$. Notice that in this equation the original count of the GFP is not multiplied by any factor, and hence can be directly compared with the solution fluorescence intensity.

The second procedure employed to evaluate the surface intensity was to use a bleached crystal as a reference. In this method, the fluorescence signal from a crystal is bleached to 1% of its original value. The percentage of liquid in the detection volume at the peripheral ice region is then determined using

$$C_2 = \frac{(\bar{I}_{\text{Bleached Crystal}} - B_{\text{GFP}})}{(\bar{I}_{\text{Solution}} - B_{\text{GFP}})}. \qquad (2)$$

Then, using the C_2 value obtained from Eq. 2, we determined the surface intensity of the same crystal at other times with

$$\bar{I}_{\text{subtraction2}} = (\bar{I}_{\text{Crystal}} - B_{\text{GFP}}) - C_2 \times (\bar{I}_{\text{Solution}} - B_{\text{GFP}}). \qquad (3)$$

The two methods gave comparable results, and were used according to whether a bleached crystal or Cy5 images were available in a particular experiment.

The fluorescence recovery after photobleaching (FRAP) experiments

Ice crystals in GFP-AFP solution were imaged within the thermal hysteresis temperature range. A whole ice crystal or part of it was exposed to 488 nm illumination for several minutes until its fluorescence was reduced to low levels. The crystal was then reimaged at time intervals of 1 h. Finally, the crystal was slightly melted back by briefly raising the temperature of the cell, then regrown to approximately its original size and shape by cooling the cell, and after that imaged again. The images were processed as described above to

subtract the fluorescence from the free protein in solution, and the intensity from the bipyramidal part of the crystal was plotted as a function of time.

RESULTS

Visualization of ice growth in the GFP-AFP solution

A solution in a thin cell containing GFP-AFP (0.3–3 mg/mL) in buffer (pH 8.0, 10 mM Tris-HCl, 1 mM EDTA, and 5 mM ammonium bicarbonate) and 1 μM Cyanine 5-dUTP (PerkinElmer, Shelton, CT) was cooled to low temperature. The solutions spontaneously nucleated between -15°C and -35°C and then rapidly froze. This ice was melted back and regrown by manipulating the temperature until it consisted of separate, single-crystal grains a few microns in diameter. During very slow cooling within the thermal hysteresis gap, these crystals grow into bipyramidal shapes (Fig. 3), after which visible growth stops and the crystals become stable. Thus the crystals were produced in two stages, which we refer to as initial ice (core) and new ice (see Fig. 3 *B*1). Introducing crystals into a solution by enforced freezing followed by controlled melting has been used in a standard procedure for measuring antifreeze activity over the last 35 years (i.e., thermal hysteresis measurements using a nanoliter osmometer (54)) and is a useful tool for generating a limited number of ice crystals in solution in a tiny space, such as in the present experimental cell.

In Fig. 3 *B*1 it can be seen that the core is bright and has fine features within it. This initial ice originates from ice growth at temperatures below the equilibrium freezing temperature. At these temperatures, small ice crystals grow in the *C*-direction (parallel to the *c*-axis) and emerge from each other producing finely textured ice comprised of small crystals that are all oriented in the same way. These crystals are covered by GFP-AFPs, and fluoresce brightly. After being melted to a small grain, these bright crystals form the core of a bipyramid.

Relative to the core, the new ice has lower fluorescence. We find that the core is 3 ± 1 ($n = 90$) times brighter than the fluorescence of the peripheral new ice. The bipyramidal shape emerges from controlled growth that is arrested by attachment of the AFP to the pyramidal surfaces. Analysis of the image indicates that the AFPs associated with the new ice are bound to its surface only, and are not engulfed as the crystal grows, because the fluorescence signal is not increased in the areas closer to the center where the thickness of the crystal is greater.

The GFP-AFP conjugated molecules are present in solution and on the ice surfaces. The illuminated volume contains ice, solution, and the ice/solution interface. To separate the contributions to the fluorescence of the free molecules in solution and the ice-bound molecules, ice crystals were grown in a solution containing the GFP-AFP conjugate as well as a second dye that is not conjugated to AFP, Cy5-dUTP. In this approach, the background is reduced by subtracting the image of the nonconjugated dye from the GFP-AFP image. As can be seen in Fig. 3 *B*3, the nonconjugated dye does not adhere to the ice surface and is not incorporated into the bulk ice. A crystal that has a very bright fluorescence originating from GFP exhibits no Cy5 fluorescence. The green-scale image in Fig. 3 *B*4 displays the outcome of the subtraction of the image captured through the Cy5 filter from the image captured through the GFP filter. This result shows only GFP-AFP on and within the ice crystal, and the distribution of fluorescence clearly shows that GFP-AFP adheres to the ice.

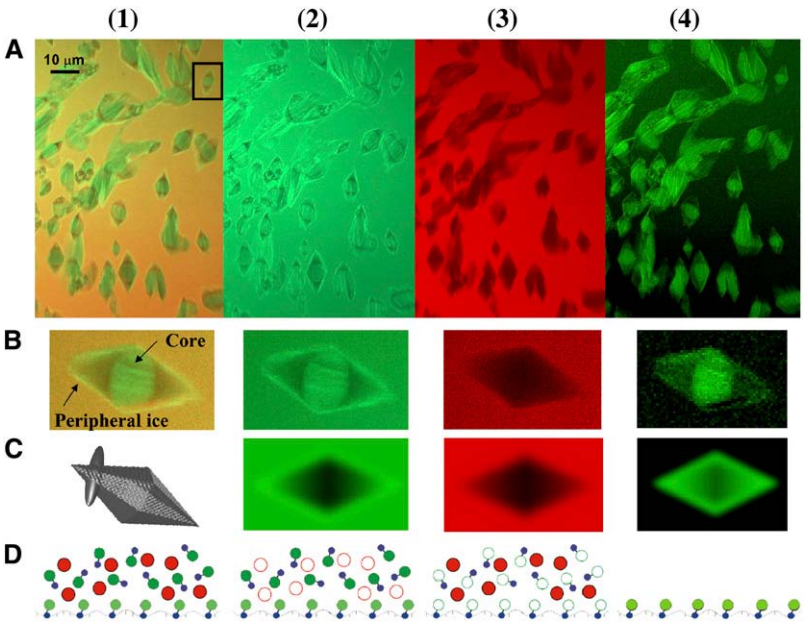

FIGURE 3 Ice crystals in the presence of GFP-AFP type III. Ice crystals were produced in a solution containing GFP-AFP and a free dye (Cy5-dUTP) and imaged with 488 nm and 633 nm illumination lines through two separate fluorescence filters (a Cy5 filter and a GFP filter). Row *A* displays images of ice crystals representing (A1) both GFP and Cy5 fluorescence; (A2) GFP fluorescence; (A3) Cy5 fluorescence; and (A4) subtraction of the Cy5 image from the GFP image according to Eq. 1. Row *B*: Magnified image of the boxed crystal in A1. (B1) The bright fluorescence in the middle of the crystal (core) corresponds to ice formed during the fast growth phase, whereas ice grown slowly during reshaping to the bipyramidal structure (peripheral ice) has lower fluorescence intensity. Row *C*: Model of the bipyramidal ice crystal shape and a three-dimensional Gaussian PSF (C1) and the convolutions between them: (C2) weighted sum of surface and solution, (C3) solution only, and (C4) crystal only. These simulations did not include the contribution from the core. Row *D* shows the molecules that are present: GFP, green circles; and Cy5, red circles. Solid circles represent molecules detected by fluorescence with a particular optical filter and open circles denote molecules that are not detected. AFP domains are blue.

The fact that a bright core appears only for GFP-AFP molecules and not for Cy5 molecules excludes the possibility that the fluorescence in the core results from trapped solution, and confirms that it results from protein attachment to the ice surfaces via AFP-specific affinity at the initial ice formation stage.

Control experiment: unconjugated GFP does not associate with or become included in ice

To verify that GFP does not adhere to ice, as it does with some crystals (55), and to verify the subtraction method, a solution containing untagged AFP, unconjugated GFP, and a second free dye, dUTP-Cy5, was frozen as described above. The images produced by the Cy5 and GFP filters are similar, with a uniform, bright background surrounding a dark crystal (Fig. 4, *A* and *B*). The gradual variation in the fluorescence intensity from the level in the solution to the absence of fluorescence in the middle of the crystal is consistent with the fraction of the detection volume occupied by ice. The subtraction of the Cy5 fluorescence from that of GFP confirmed that there was virtually no difference between the distributions of these two molecules (Fig. 4, *C* and *D*). Thus this experiment shows that GFP neither adheres to the ice surface nor becomes incorporated into the bulk, and establishes that the signal observed from the ice surfaces with conjugated GFP-AFP results from the activity of the AFP moiety.

Estimation of the surface density of the bound GFP-AFPs

To test our assumption that the measured signal derives from a single layer of bound proteins, and to measure their surface density, we modeled the signal as a convolution of the point spread function (PSF) with the shape that resembles the crystal surface. By comparing the ratio of the experimental signal from the AFP-GFP solution to the experimental signal due to the bound molecules on the surface with the ratio of the modeled signals, we could determine the surface density of the AFP on the ice surface. As will be shown below, our results are consistent with the presence of a single layer of bound proteins on the ice surface. The details of the model are described below.

The effective detection PSF is assumed to be a Gaussian function (52) of the form

$$PSF(x,y,z) = \exp\left[-\left(\frac{x^2+y^2}{w_l^2}+\frac{z^2}{w_a^2}\right)\right], \tag{4}$$

where w_l and w_a are the lateral and axial widths, which are equal to lateral/axial $(1/(2\times\sqrt{\ln 2}))$ *FWHM*. Thus the signal from a uniform concentration of fluorescent molecules in the solution within the detection volume is

$$\begin{aligned} I_{\text{solution}} &= \iiint CI_{\text{GFP}} \cdot PSF(x,y,z)dxdydz \\ &= CI_{\text{GFP}} \times \pi^{3/2} w_l^2 w_a, \end{aligned} \tag{5}$$

where C is the concentration of GFP-AFP in the solution and I_{GFP} is the signal from a single GFP molecule at the center of the illumination. The signal from the surface is the lateral convolution of the PSF with the crystal surface,

$$\begin{aligned} I_{\text{surface}}(x,y) = \sigma \times I_{\text{GFP}} \times \iiint PSF(x'-x, y'-y, z') \\ \cdot S(x',y',z')\frac{dx'dy'dz'}{\Delta} = \sigma \times I_{\text{GFP}} \times \Delta^2 \times Conv, \end{aligned} \tag{6}$$

where σ is the surface density of the bound GFP-AFP, which is assumed to be constant over the surface of the crystal, $S(x',y',z')$ is a function that equals one at the surface of a bipyramidal polyhedral and zero elsewhere, *Conv* is the value of the integral in Δ^2 units, and Δ is the grid spacing over which the calculation is performed.

Dividing Eq. 6 by Eq. 5 and averaging over the peripheral ice area yields the surface density

$$\sigma = \frac{\langle I_{\text{surface}}\rangle}{I_{\text{solution}}} \times \frac{\pi^{3/2} w_l^2 w_a}{\Delta^2 \langle Conv\rangle} \times C. \tag{7}$$

To evaluate $\langle Conv\rangle$ and test our interpretation of the experimental data, we modeled the bipyramidal polyhedron and the Gaussian PSF with subroutines written by our group in the IDL software platform (RSI, Boulder, CO). Within a

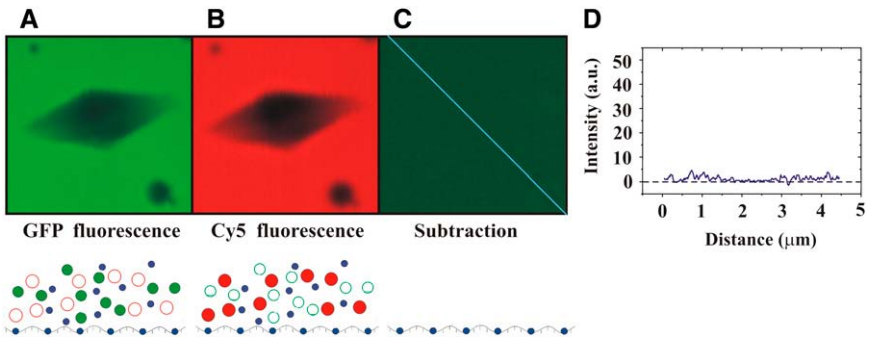

FIGURE 4 Unconjugated GFP does not accumulate within or on the surface of ice crystals. An ice crystal was grown in a solution containing AFP, unconjugated GFP, and Cyanine 5-dUTP. The ice crystal was illuminated with 488 nm and 633 nm lasers and imaged through a GFP filter (*A*) and through a Cy5 filter (*B*). For both filters the crystal appears dark. Panel *C* shows the outcome of the subtraction of the I_{Cy5} image from the I_{GFP} image. The intensity of fluorescence along the blue line in the subtracted image is displayed in the graph (*D*). The lower parts of panels (*A–C*) show the molecules that are present as described in the caption for Fig. 3.

matrix ($300 \times 300 \times 300$) that represents an $(18.75\ \mu m)^3$ volume with a grid spacing of $\Delta = 62.5$ nm, we constructed a 10-μm long bipyramidal shape. We assigned a value of one to voxels on its surface, and zero at all other locations. This matrix thus represents the surface of the crystal. In a second matrix of the same dimensions, we assigned a value of one to all points outside the bipyramidal shape and zero to all points within the shape and on its surface. This second matrix thus represents the solution outside the crystal. In addition, we constructed a matrix with a three-dimensional Gaussian function according to the given PSF formula using widths determined in the experiments. The crystal shape and the Gaussian PSF are illustrated in Fig. 3 *C*1. Next we laterally convolved the PSF matrix with each of the crystal matrices. A weighted sum of the convolutions of the two matrices is shown in Fig. 3 *C*2. This sum represents the signal from the GFP at the surface and in solution, but without the contribution from the core. Fig. 3 *C*2 is colored green to emphasize the similarity between these results and the GFP images (Fig. 3 *B*2). The convolution with the solution matrix is shown in Fig. 3 *C*3. This convolution, which represents the contribution from the solution only, is colored red to emphasize its similarity to the results for the Cy5 contribution (Fig. 3 *B*3). The convolution with the crystal shell matrix is shown in Fig. 3 *C*4. This convolution, which represents the surface contribution, is shown on a green scale to emphasize its similarity to the subtraction images (Fig. 3 *B*4). We average the tip area of the convolution in Fig. 3 *C*4 to evaluate the value of $\langle Conv\rangle \times \Delta^2 = 240 \times \Delta^2 = 0.94\ \mu m^2$. To validate our algorithm, we compared the value of the convolution with the solution area in Fig. 3 *C*3 to the analytical value of the PSF effective volume, $\pi^{3/2} w_l^2 w_a = 9645 \times \Delta^3 = 2.357\ \mu m^3$, where the PSF widths are set to be $w_l = 0.42$ and $w_a = 2.4$ according to the experimental measurement of the PSF (see Materials and Methods and Eq. 4). The deviation from the analytical value was $<0.1\%$, indicating that no artifacts are introduced in the construction of the matrices and the convolution. When we repeated the calculations using a smaller grid size, $\Delta = 50$ nm, we obtained approximately the same result for the relevant ratio, which is the effective volume of the detection divided by the effective illuminated surface of the crystal, $(\pi^{3/2} w_l^2 w_a / \Delta^2 \langle Conv\rangle) = 2.510 \pm 0.003\ \mu m$, indicating that the grid spacing is small enough for our calculation needs. From experimental measurements of the surface intensity and solution intensity, we found that $(I_{solution}/I_{surface}) = 9.3 \pm 0.7$ ($n = 90$). Finally, from the thermal hysteresis activity (46), we estimated the protein concentration in the solution to be $C = 15 \pm 5\ \mu M$. Using this data in Eq. 7 allowed us to calculate a GFP-AFP surface density of $\sigma = 2400 \pm 900$ molecules/μm^2, which corresponds to an average spacing between adsorbed GFP-AFP molecules of 20 ± 5 nm. This separation is consistent with a previous estimate for antifreeze glycoprotein (43) and supports our assumption that the signal arises from a single layer of bound GFP-AFP.

Quasi-permanent binding of AFPs to ice demonstrated by absence of recovery after photobleaching

Fluorescence recovery after photobleaching (FRAP) has been widely used to monitor dynamic molecular processes (49,56,57). We used this method to determine the limit on the recovery of the fluorescence signal from ice-bound molecules. In these experiments, protein molecules bound to the ice surface were photobleached, and then the intensity of fluorescence from the surface was monitored to detect the replacement of the bleached molecules with unbleached molecules from the surrounding solution.

In the FRAP experiments, ice crystals decorated with AFP-GFP were monitored for several hours at a constant temperature that was 0.2°C below the melting point of the crystals ($T_{experiment} = -0.64 \pm 0.02$°C, $T_{melting} = -0.42 \pm 0.02$°C). The regions of AFP-decorated ice crystals were divided into two groups. One region was bleached by 60 successive exposures to 100% of the 488 nm laser power (0.12 mW at the objective entrance) of the confocal microscope with 100 μs per pixel and a pixel size of 130 nm. Under these conditions, the fluorescence intensity from the core and peripheral ice dropped by 8% per scan. Thus the fluorescence signal was bleached down to $<1\%$ of its initial value. Thereafter, the crystals were imaged every hour by 50% laser power and 50 μs per pixel with the same pixel size. Thus the bleaching per scan was 2%. Fig. 5 shows a series of representative images from such experiments. In this experiment, the proteins on half of the surface of each crystal are bleached, leaving the other half of the crystal as a control region of unbleached GFP-AFP on peripheral ice. The surface intensity was calculated using Eq. 3. The value of C_2 in Eq. 3, which represents the solution fraction in the detection volume over the area of the peripheral ice, was typically $\sim 65\%$. The signal was averaged using results from several crystals in several independent experiments (see Fig. 6 legend for details).

Over a period of up to 20 h, there was no recovery of fluorescence above the limit of resolution (Fig. 6). This demonstrates that there is no detectable overgrowth of the bound AFPs during this period. If the AFPs were overgrown, the supercooled crystal would not remain stable unless fresh (unbleached) GFP-AFPs adsorbed onto the newly formed layer of ice. Moreover, the lack of recovery also indicates that there is no detectable exchange of bound protein with free protein in the solution, which suggests that GFP-AFP is permanently bound to the ice. If the binding of the GFP-AFP was in equilibrium and bound protein could exchange with the protein in the solution, the bleached GFP-AFP would be replaced by the excess free unbleached GFP-AFP in the solution surrounding the crystal and the fluorescence signal would recover. The diffusion of GFP-AFP in the solution is sufficiently fast to assume that the amount of bleached free protein is negligible near a stable crystal (see Appendix).

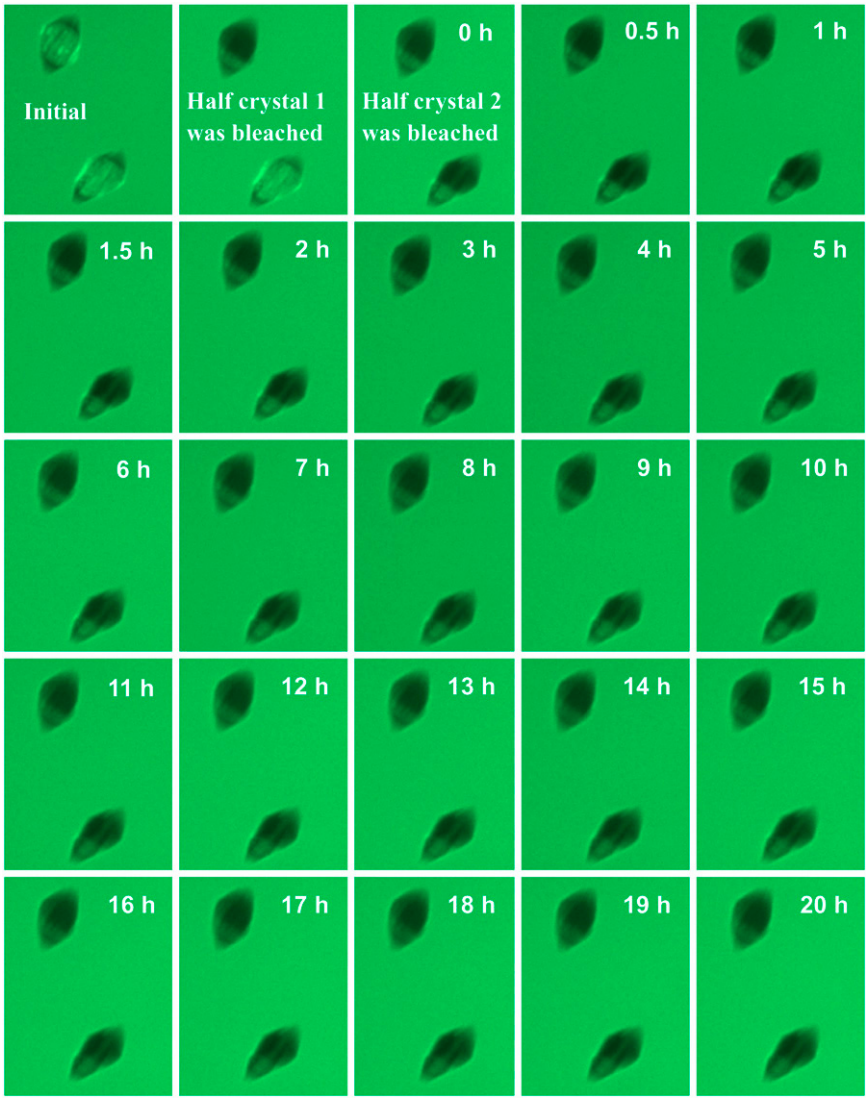

FIGURE 5 FRAP experiment. Confocal images of crystals recorded over 20 h. For each of the displayed crystals, half of the crystal was bleached and half was left unbleached. The intensities of the bleached and unbleached parts were monitored as a function of time for a period of 20 h. The average signals from the bleached parts of ~20 crystals, as well as those from the unbleached parts, are shown in Fig. 6.

Furthermore, we monitored the intensity of fluorescence near the crystal and determined that the level of unbleached GFP-AFP molecules in solution did not change. The control group of crystal regions that were not bleached and were imaged in parallel to the bleached group showed a signal intensity reduction to the level of ~75% of the initial intensity, as expected from their exposure to ~15 cycles of illumination causing 2% bleaching per exposure (see Fig. 6).

If undetectable slow exchange or engulfment is occurring, we can estimate the upper limit of its timescale by assuming that it is marginally detected in our experiments. To estimate the possible exchange time, we compare the experimental data to the results provided by a rate equation. We assume that the bound molecule leaves the surface or is engulfed within some characteristic slow timescale $1/k_{\mathrm{off}}$ and then, shortly afterwards, before the crystal grows significantly, it is replaced by an unbleached molecule from the solution. We take into account the amount of bleaching induced by the light source during imaging, α_{i}, and so

$$C_{\mathrm{i+1}} = C_{\mathrm{i}} + (100 - C_{\mathrm{i}})k_{\mathrm{off}} \times (t_{\mathrm{i+1}} - t_{\mathrm{i}}) - C_{\mathrm{i}}\alpha_{\mathrm{i}}\delta_{\mathrm{i}}, \qquad (8)$$

where C is the percentage of bound unbleached molecules. The percentage of bleached molecules is thus $100 - C$, since we assume that all docking positions are occupied as the adsorption is quasi-permanent. The value $\alpha_{\mathrm{i}} = 2\%$ is the percentage of bleaching during a single observation and δ_{i} equals one when an observation occurs and zero otherwise. Fig. 6 shows the results of this kinetic model for the bleached and unbleached molecules for a time constant of seven days, and also for the bleached molecules for a time constant of one day. The data clearly show that the signal corresponds to a recovery time of longer than one week. Thus we estimate that a recovery time of one week yields a signal on the

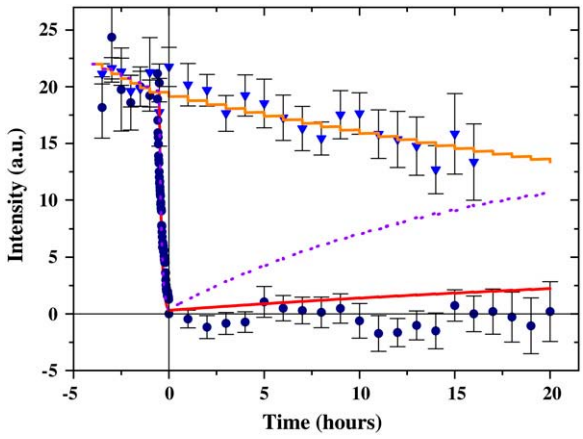

FIGURE 6 Absence of exchange of ice-bound fluorescent antifreeze proteins after photobleaching. This graph shows the results from the FRAP experiments. The surface intensities of the bleached (*circles*) and unbleached (*triangles*) regions of crystals were calculated according to Eq. 3 and displayed as a function of time. Kinetic models of the recovery of the fluorescence signal after photobleaching with recovery periods of one day (*purple line*) and seven days (*red line* for *bleached* and *orange line* for *unbleached*) are also shown. Bleaching of 2% per observation is included in the model. The data were averaged over several crystals in four separate experiments. The number of crystals n at each time window was ($0 \le t \le 14$ h, $20 \le n \le 27$), ($5 \le t \le 14$ h, $17 \le n \le 19$), and ($15 \le$ t ≤ 20 h, $9 \le n \le 14$) for the bleached regions; and ($0 \le t \le 10$ h, $n = 12$), ($11 \le t \le 14$ h, $9 \le n \le 10$), and ($15 \le t \le 16$ h, $n = 2$) for the unbleached regions.

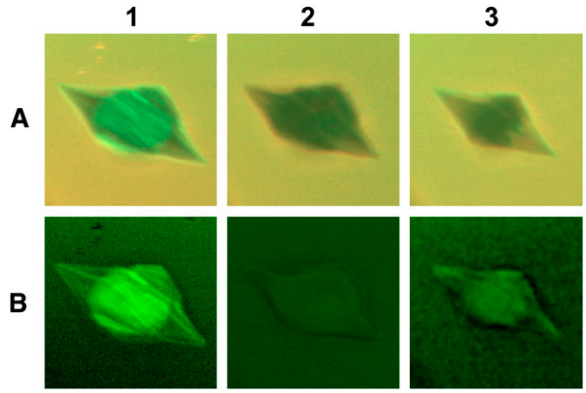

FIGURE 7 Photobleaching and recovery after reshaping of ice. Row *A* contains the summation of GFP and Cy5 fluorescence images of an ice crystal as in Fig. 3 *A*1. Row *B* shows the corresponding subtracted images as described in Eq. 1 and Fig. 3 *A*4. Column 1 corresponds to the initial image before bleaching. Column 2 corresponds to the crystal after photobleaching. The fluorescence intensity did not recover within the experimental period of several hours (see Fig. 6). Column 3 corresponds to the same crystal after it had been warmed to slightly above its melting temperature and then cooled to allow reshaping to the bipyramidal shape. GFP-AFP was found to accumulate on the newly formed surfaces of the crystal.

order of our experimental uncertainty, and thus the experimental limit for the exchange or engulfment constant is one week.

To demonstrate that our methodology is capable of detecting the renewal of bound GFP-AFP on an ice surface, in most of our experiments we warmed the solution until the crystals had partially melted and then cooled the solution and regrew the crystals ($n = 21$). GFP-AFP was found to accumulate on the newly formed surfaces of the resulting crystals, as shown in the representative example in Fig. 7. In most cases, the intensity returned to a value slightly below that before bleaching.

The growth rate of protected ice crystals is assumed to be zero, as found from observation of crystals for long periods (22). Assuming a resolution of 0.7 μm in such measurements and a time frame as long as one week, the optical microscopy results indicate an upper limit on the growth rate of ~100 nm/day. As discussed above, our experiments indicate a lower limit of seven days for recovery. If this limit represents the rate of engulfment, and we assume that 10 nm of ice is needed to cover the protein layer, then the upper limit of growth rate is 1.4 nm/day, which is an improvement by more than an order of magnitude over previous estimates. At such a rate, very few molecules will be covered every second by the ice, out of the ~1,000,000 molecules that are bound to a crystal that is a few micrometers in diameter with a surface density of a few thousand molecules/μm^2.

DISCUSSION AND CONCLUSIONS

Our approach circumvents the principal difficulty of working with AFPs, namely that their binding to ice can only be assessed indirectly through observations of ice crystal growth and morphology. The theory that AFPs bind irreversibly to specific ice surfaces and thus cause facet formation, and that ice growth is completely stopped on these surfaces, has been proposed (22,30,31,34) but not directly verified. One opposing viewpoint suggests that AFPs bind reversibly and do not stop ice growth entirely, but nonetheless suppress the growth rate sufficiently to avoid detection. Yet another hypothesis attributes AFP activity to the colligative effect of a high local concentration established by equilibrium binding to the ice surface (42). An apparent drawback to this latter hypothesis is that even a modest freezing point depression of 0.5°C would require the local concentration of solutes to be >0.25 M, which corresponds to 300 mg/mL for Type I AFP, assuming three counterions per protein molecule. To achieve a thermal hysteresis activity of 1°C through the colligative properties of Type III AFPs, a local concentration of 1200 mg/mL would be required. Furthermore it is not clear how a gradient of AFP can be supported, given the lack of long distance attraction between the AFPs and the crystal. The current understanding of the interaction between AFPs and ice surfaces is that close proximity between the AFP molecules and ice surface is required. The lack of recovery of fluorescence after photobleaching clearly supports the adsorption-inhibition model. If the ice surface were to grow, every newly added layer of water molecules would require a new coating of antifreeze proteins, which would be drawn from the pool of unbleached GFP-AFP in solution, thereby

restoring the fluorescence signal. Likewise, if AFP binding were reversible, bleached proteins would be exchanged with unbleached proteins and the surface would regain its fluorescence. No such recovery was observed, and our results allow for only occasional engulfment or exchange of individual molecules. If these rare events do occur, they might be important in explaining the variation of thermal hysteresis with concentration (24). Further investigation with increased sensitivity will be needed to detect such minute degrees of growth.

Spin exchange NMR (42) has been used to determine that the timescale of exchange of Type I AFPs is 1 s, but it is not clear if the signal used in this approach originated from molecules that Ba et al. (42) claim accumulate at the ice-water interface and protect the ice from freezing. Other attempts to investigate AFP binding kinetics on ice crystals (43,58–60) have suffered from low sensitivity and were not able to determine the off-rates of the proteins. The ice hemisphere etching technique (31) enables the determination of the preferred binding planes of AFPs on ice, but does not directly reveal the kinetics of attachment. Ellipsometry and related methods have been used to measure the accumulation of AFPs on ice surfaces (43), but cannot reveal the detachment timescale, and these experiments were carried out on large scale ice and not on micron-size crystals that are covered with AFP molecules. Fluorescent tagging is an ideal method for visualizing AFPs in action because the emitted light can be transmitted through ice. The intensity of the signal is proportional to the amount of AFP present, and by observing the recovery of the fluorescence signal after photobleaching, the exchange of adsorbed molecules can be detected.

Experiments with fluorescently tagged macromolecules that adhere to calcium tartrate crystals (47) have shown that a large refractive index difference between the crystal and the surrounding solution can cause internal reflection of the signal, which could lead to misinterpretation of the position of the adsorbed molecules. However, the difference in refractive index between supercooled water and ice is only 3% (61,62), and so substantial internal reflection is not expected to occur.

There are a number of considerations in the choice of which AFP to label. Of primary importance is ensuring that the attachment of the large (27 kDa) GFP molecule does not compromise the effectiveness of the antifreeze protein. Such problems are likely to occur with the α-helical Type I AFPs from flounder or sculpin, in which the N- and C-termini are in the same plane as the ice-binding site. Attachment of a bulky globular protein at either end of such an AFP is likely to sterically hinder the engagement of its binding site to ice. Further, these termini should not be modified because they are involved in helix capping interactions, and in some cases are post-translationally modified to facilitate this structural stabilization (63). The extensively disulfide-bonded AFPs from insects and fish (Type II AFPs) are extremely difficult to produce and correctly refold even without the complication of attaching an additional domain. Finally, antifreeze glycoproteins have not yet been produced biosynthetically. Thus Type III AFPs were preferred for labeling in this manner because their N- and C-termini are on the other side of the proteins from their ice-binding sites (45). The feasibility of making active fusion proteins with Type III AFPs has previously been established in thioredoxin and maltose-binding protein fusions. While one might expect that other types of AFPs act on ice through similar irreversible adsorption mechanisms, the experimental verification of this mechanism might require a method for labeling them with a photobleachable tag that does not impair ice binding.

One of the surprising results of our use of Type III AFP-GFP fusion is the intensity with which the cores of the ice crystals become fluorescently labeled. This happens when GFP-AFP becomes incorporated into the crystals during the initial rapid freezing of the solution. The ice core retains this label when the ice is melted back to obtain single crystals. Incorporation also happens when the crystal grows rapidly at moderate supercooling below the nonequilibrium freezing temperature. We suggest that the growth of these ice crystals parallel to the *c*-axis increases the primary prism-plane surface area available for binding. Although the work of Antson et al. (33) shows that Type III AFPs will also bind to certain pyramidal planes, it is not clear if these planes are expressed during the rapid growth phase. The incorporation of GFP-AFP is clearly due solely to the attached AFP, because GFP is not incorporated by itself into the ice crystal during freezing but is totally excluded as expected for any non-AFP (Fig. 4 *A*). After melting back and controlled regrowth to form a hexagonal bipyramidal crystal, the proteins adhere to the ice surface, but could in principle adhere to primary prism planes parallel to the *c*-axis and then be engulfed during bipyramidal crystal growth. The observation that the fluorescence intensity does not increase with the thickness of the crystal present in the detection volume shows that GFP-AFP is not found within the newly formed tips of the bipyramid, but is only bound to the surface. This is consistent with the surface-active role of the AFP in stopping growth of ice on the binding planes, but does not distinguish between a model of stepwise growth inhibition at the junction of the prism and basal planes (45) versus one in which AFP stops ice growth by binding to specific pyramidal planes (33).

In summary, the use of a fluorescently tagged Type III AFP and targeted photobleaching has enabled us to visualize the binding of the AFP to the surface of ice and provided the first direct demonstration that 1), binding is quasi-permanent, i.e., the AFP molecule stays on the surface for more than seven days; and 2), the AFPs are not overgrown by the ice front at temperatures within the thermal hysteresis gap other than in possible rare events that result in growth of <2 nm/day. The remarkable variation in protein structure, ice shaping morphology, and thermal hysteresis activity of the various types of AFPs might be due to variations in the mechanism of inhibition. If so, these could be resolved by extension of this research.

APPENDIX

Fluorescence and bleaching rates of GFP-AFP in solution and in ice

In our experiments examining GFP fluorescence and bleaching in a frozen environment, we used a wide field epifluorescence microscope (Nikon TE2000) equipped with an argon laser and a fluorescence filter set that included a trichroic beam splitter and emission filter set (488/543/633 nm, Chroma, Rockingham, VT).

We checked the relative fluorescence of GFP-AFP within the ice and in solution. We froze the whole sample and measured the average intensity of a full field of view with a low laser intensity that does not bleach the sample significantly in the time of observation. We then melted this ice and again measured the intensity; we found the same average signal. Thus we conclude that GFP-AFP fluorescence is not dependent on whether the water is in the liquid or solid phase. This finding might be different for dyes that are more sensitive to their local environment (64).

We checked whether the bleaching rate in ice would be slower than in water, since it is possible that oxygen mobility might influence bleaching. We completely froze a GFP-AFP sample and then bleached it with a laser power of 40 mW and a 120-μm diameter field of view. The sample bleached on a timescale of 6.5 min (e^{-1}) and stayed dark thereafter. To measure the bleaching time of GFP-AFP in solution while minimizing diffusion effects, we located a trapped solution pool of a size of 15 μm $\times$ 15 μm in a partially frozen sample, and monitored its bleaching with the same illumination intensity. We found that the bleaching rate of GFP-AFP in solution was the same as that in ice.

Diffusion of GFP-AFP in solution

We estimate that the diffusion coefficient of GFP-AFP molecules in 0°C solution is $D = 55\ \mu m^2/s$. This estimate is based on the equation $D = (kT/6\pi a\eta)$ in Berg (65), where k is Boltzmann's constant, T is the temperature in Kelvin, $a = 2$ nm which is the effective radius of the GFP-AFP molecule, and $\eta = 1.8 \times 10^{-3}\ N \times s/m^2$, the viscosity of water at 0°C. The diffusion coefficient of a single molecule of GFP was measured in viscous solution, and was found to be in agreement with the theoretical estimate (66). We tried to directly bleach a 120-μm diameter area of GFP-AFP solution close to the melting point temperature, but only a slight diminution of the signal was found. Our interpretation is that the diffusion of unbleached molecules from the surroundings replenishes the bleached molecules in the illuminated area. Indeed the bleaching time of 6.5 min is much longer than the diffusion time for the radius of 60 μm, $\tau_D = \frac{r^2}{4D} = 16$ s, and thus bleached molecules do not accumulate in the illumination area.

We thank S. Gauthier and R. Milford for their assistance. This study was supported by the Canadian Institutes for Health Research, the Bosack and Kruger Foundation, the National Science Foundation (grant Nos. OPP0440841, OPP0439805, and OPP0135989), the Condensed Matter and Surface Science program at Ohio University, (grant Nos. OPP0440841, OPP0439805, and OPP0135989) the Ohio University's NanoBioTechnology Initiative.

REFERENCES

1. Davies, P. L., J. Baardsnes, M. J. Kuiper, and V. K. Walker. 2002. Structure and function of antifreeze proteins. *Philos. Trans. R. Soc. Lond. B Biol. Sci.* 357:927–935.
2. Yeh, Y., and R. E. Feeney. 1996. Antifreeze proteins: structures and mechanisms of function. *Chem. Rev.* 96:601–618.
3. Ewart, K. V., Q. Lin, and C. L. Hew. 1999. Structure, function and evolution of antifreeze proteins. *Cell. Mol. Life Sci.* 55:271–283.
4. DeVries, A. L. 1971. Glycoproteins as biological antifreeze agents in Antarctic fishes. *Science.* 172:1152–1155.
5. Tomchaney, A. P., J. P. Morris, S. H. Kang, and J. G. Duman. 1982. Purification, composition, and physical properties of a thermal hysteresis ''antifreeze'' protein from larvae of the beetle, *Tenebrio molitor*. *Biochemistry.* 21:716–721.
6. Graham, L. A., and P. L. Davies. 2005. Glycine-rich antifreeze proteins from snow fleas. *Science.* 310:461.
7. Urrutia, M. E., J. G. Duman, and C. A. Knight. 1992. Plant thermal hysteresis proteins. *Biochim. Biophys. Acta.* 1121:199–206.
8. Worrall, D., L. Elias, D. Ashford, M. Smallwood, C. Sidebottom, P. Lillford, J. Telford, C. Holt, and D. Bowles. 1998. A carrot leucine-rich-repeat protein that inhibits ice recrystallization. *Science.* 282:115–117.
9. Gilbert, J. A., P. J. Hill, C. E. Dodd, and J. Laybourn-Parry. 2004. Demonstration of antifreeze protein activity in Antarctic lake bacteria. *Microbiology.* 150:171–180.
10. Muryoi, N., M. Sato, S. Kaneko, H. Kawahara, H. Obata, M. W. F. Yaish, M. Griffith, and B. R. Glick. 2004. Cloning and expression of afpA, a gene encoding an antifreeze protein from the arctic plant growth-promoting rhizobacterium *Pseudomonas putida* GR12–2. *J. Bacteriol.* 186:5661–5671.
11. Robinson, C. H. 2001. Cold adaptation in Arctic and Antarctic fungi. *New Phytol.* 151:341–353.
12. Huang, T., J. Nicodemus, D. G. Zarka, M. F. Thomashow, M. Wisniewski, and J. G. Duman. 2002. Expression of an insect (*Dendroides canadensis*) antifreeze protein in *Arabidopsis thaliana* results in a decrease in plant freezing temperature. *Plant Mol. Biol.* 50:333–344.
13. Hew, C., R. Poon, F. Xiong, S. Gauthier, M. Shears, M. King, P. Davies, and G. Fletcher. 1999. Liver-specific and seasonal expression of transgenic Atlantic salmon harboring the winter flounder antifreeze protein gene. *Transgenic Res.* 8:405–414.
14. Griffith, M., and K. V. Ewart. 1995. Antifreeze proteins and their potential use in frozen foods. *Biotechnol. Adv.* 13:375–402.
15. Breton, G., J. Danyluk, F. Ouellet, and F. Sarhan. 2000. Biotechnological applications of plant freezing associated proteins. *Biotechnol. Annu. Rev.* 6:59–101.
16. Rubinsky, B., A. Arav, and A. L. DeVries. 1992. The cryoprotective effect of antifreeze glycopeptides from Antarctic fishes. *Cryobiology.* 29:69–79.
17. Li, B., and D. W. Sun. 2002. Novel methods for rapid freezing and thawing of foods—a review. *J. Food Eng.* 54:175–182.
18. Jia, Z., and P. L. Davies. 2002. Antifreeze proteins: an unusual receptor-ligand interaction. *Trends Biochem. Sci.* 27:101–106.
19. Graether, S. P., C. M. Slupsky, P. L. Davies, and B. D. Sykes. 2001. Structure of type I antifreeze protein and mutants in supercooled water. *Biophys. J.* 81:1677–1683.
20. Graether, S. P., M. J. Kuiper, S. M. Gagne, V. K. Walker, Z. Jia, B. D. Sykes, and P. L. Davies. 2000. Beta-helix structure and ice-binding properties of a hyperactive antifreeze protein from an insect. *Nature.* 406:325–328.
21. Scotter, A. J., C. B. Marshall, L. A. Graham, J. A. Gilbert, C. P. Garnham, and P. L. Davies. 2006. The basis for hyperactivity of antifreeze proteins. *Cryobiology.* 53:229–239.
22. Raymond, J. A., and A. L. DeVries. 1977. Adsorption inhibition as a mechanism of freezing resistance in polar fishes. *Proc. Natl. Acad. Sci. USA.* 74:2589–2593.
23. Knight, C. A. 2000. Structural biology: adding to the antifreeze agenda. *Nature.* 406:249–251.
24. Knight, C. A., and A. Wierzbicki. 2001. Adsorption of biomolecules to ice and their effects upon ice growth. 2. A discussion of the basic mechanism of ''antifreeze'' phenomena. *Cryst. Growth Des.* 1:439–446.
25. Sonnichsen, F. D., C. I. DeLuca, P. L. Davies, and B. D. Sykes. 1996. Refined solution structure of type III antifreeze protein: hydrophobic groups may be involved in the energetics of the protein-ice interaction. *Structure.* 4:1325–1337.

26. Harding, M. M., L. G. Ward, and A. D. Haymet. 1999. Type I ''antifreeze'' proteins. Structure-activity studies and mechanisms of ice growth inhibition. *Eur. J. Biochem.* 264:653–665.
27. Yang, D. S., W. C. Hon, S. Bubanko, Y. Xue, J. Seetharaman, C. L. Hew, and F. Sicheri. 1998. Identification of the ice-binding surface on a type III antifreeze protein with a ''flatness function'' algorithm. *Biophys. J.* 74:2142–2151.
28. Doxey, A. C., M. W. Yaish, M. Griffith, and B. J. McConkey. 2006. Ordered surface carbons distinguish antifreeze proteins and their ice-binding regions. *Nat. Biotechnol.* 24:852–855.
29. Sander, L. M., and A. V. Tkachenko. 2004. Kinetic pinning and biological antifreezes. *Phys. Rev. Lett.* 93:128102.
30. Knight, C. A., A. L. DeVries, and L. D. Oolman. 1984. Fish antifreeze protein and the freezing and recrystallization of ice. *Nature.* 308:295–296.
31. Knight, C. A., C. C. Cheng, and A. L. DeVries. 1991. Adsorption of alpha-helical antifreeze peptides on specific ice crystal surface planes. *Biophys. J.* 59:409–418.
32. DeLuca, C. I., H. Chao, F. D. Sonnichsen, B. D. Sykes, and P. L. Davies. 1996. Effect of type III antifreeze protein dilution and mutation on the growth inhibition of ice. *Biophys. J.* 71:2346–2355.
33. Antson, A. A., D. J. Smith, D. I. Roper, S. Lewis, L. S. D. Caves, C. S. Verma, S. L. Buckley, P. J. Lillford, and R. E. Hubbard. 2001. Understanding the mechanism of ice binding by type III antifreeze proteins. *J. Mol. Biol.* 305:875–889.
34. Knight, C. A., and A. L. DeVries. 1994. Effects of a polymeric, nonequilibrium antifreeze upon ice growth from water. *J. Cryst. Growth.* 143:301–310.
35. Anklam, M. R., and A. Firoozabadi. 2005. An interfacial energy mechanism for the complete inhibition of crystal growth by inhibitor adsorption. *J. Chem. Phys.* 123:144708.
36. Hall, D. G., and A. Lips. 1999. Phenomenology and mechanism of antifreeze peptide activity. *Langmuir.* 15:1905–1912.
37. Burcham, T. S., D. T. Osuga, Y. Yeh, and R. E. Feeney. 1986. A kinetic description of antifreeze glycoprotein activity. *J. Biol. Chem.* 261:6390–6397.
38. Liu, J. J., and Q. Z. Li. 2006. Theoretical model of antifreeze protein-ice adsorption: binding of large ligands to a two-dimensional homogeneous lattice. *Chem. Phys. Lett.* 422:67–71.
39. Jorov, A., B. S. Zhorov, and D. S. C. Yang. 2004. Theoretical study of interaction of winter flounder antifreeze protein with ice. *Protein Sci.* 13:1524–1537.
40. Karim, O. A., and A. D. J. Haymet. 1988. The ice water interface—a molecular-dynamics simulation study. *J. Chem. Phys.* 89:6889–6896.
41. Wilson, P. W. 1994. A model for thermal hysteresis utilizing the anisotropic interfacial energy of ice crystals. *Cryobiology.* 31:406–412.
42. Ba, Y., J. Wongskhaluang, and J. Li. 2003. Reversible binding of the HPLC6 isoform of type I antifreeze proteins to ice surfaces and the antifreeze mechanism studied by multiple quantum filtering-spin exchange NMR experiment. *J. Am. Chem. Soc.* 125:330–331.
43. Wilson, P. W., D. Beaglehole, and A. L. DeVries. 1993. Antifreeze glycopeptide adsorption on single-crystal ice surfaces using ellipsometry. *Biophys. J.* 64:1878–1884.
44. Cubitt, A. B., R. Heim, S. R. Adams, A. E. Boyd, L. A. Gross, and R. Y. Tsien. 1995. Understanding, improving and using green fluorescent proteins. *Trends Biochem. Sci.* 20:448–455.
45. Jia, Z. C., C. I. DeLuca, H. M. Chao, and P. L. Davies. 1996. Structural basis for the binding of a globular antifreeze protein to ice. *Nature.* 384:285–288. *Correction.* 385:555.
46. DeLuca, C. I., R. Comley, and P. L. Davies. 1998. Antifreeze proteins bind independently to ice. *Biophys. J.* 74:1502–1508.
47. Zimmerman, E., B. Geiger, and L. Addadi. 2002. Initial stages of cell-matrix adhesion can be mediated and modulated by cell-surface hyaluronan. *Biophys. J.* 82:1848–1857.
48. Schnirman, A. A., E. Zahavi, H. Yeger, R. Rosenfeld, I. Benhar, Y. Reiter, and U. Sivan. 2006. Antibody molecules discriminate between crystalline facets of a gallium arsenide semiconductor. *Nano Lett.* 6: 1870–1874.
49. White, J., and E. Stelzer. 1999. Photobleaching GFP reveals protein dynamics inside live cells. *Trends Cell Biol.* 9:61–65.
50. Kuiper, M. J., C. Lankin, S. Y. Gauthier, V. K. Walker, and P. L. Davies. 2003. Purification of antifreeze proteins by adsorption to ice. *Biochem. Biophys. Res. Commun.* 300:645–648.
51. Marshall, C. B., M. E. Daley, B. D. Sykes, and P. L. Davies. 2004. Enhancing the activity of a beta-helical antifreeze protein by the engineered addition of coils. *Biochemistry.* 43:11637–11646.
52. Zhang, B., J. Zerubia, and J.-C. Olivo-Marin. 2007. Gaussian approximations of fluorescence microscope PSF models. *Appl. Optics.* 46:1819–1829.
53. Pawley, J. B. 1995. Handbook of Biological Confocal Microscopy. Plenum Press, New York.
54. Chakrabartty, A., and C. L. Hew. 1991. The effect of enhanced alpha-helicity on the activity of a winter flounder antifreeze polypeptide. *Eur. J. Biochem.* 202:1057–1063.
55. Kurimoto, M., P. Subramony, R. W. Gurney, S. Lovell, J. Chmielewski, and B. Kahr. 1999. Kinetic stabilization of biopolymers in single-crystal hosts: green fluorescent protein in alpha-lactose monohydrate. *J. Am. Chem. Soc.* 121:6952–6953.
56. Weiss, M. 2004. Challenges and artifacts in quantitative photobleaching experiments. *Traffic.* 5:662–671.
57. Klonis, N., M. Rug, I. Harper, M. Wickham, A. Cowman, and L. Tilley. 2002. Fluorescence photobleaching analysis for the study of cellular dynamics. *Eur. Biophys. J. Biophys. Lett.* 31:36–51.
58. Chapsky, L., and B. Rubinsky. 1997. Kinetics of antifreeze protein-induced ice growth inhibition. *FEBS Lett.* 412:241–244.
59. Brown, R. A., Y. Yeh, T. S. Burcham, and R. E. Feeney. 1985. Direct evidence for antifreeze glycoprotein adsorption onto an ice surface. *Biopolymers.* 24:1265–1270.
60. Furukawa, Y., N. Inohara, and E. Yokoyama. 2005. Growth patterns and interfacial kinetic supercooling at ice/water interfaces at which anti-freeze glycoprotein molecules are adsorbed. *J. Cryst. Growth.* 275:167–174.
61. Robinson, G. W., C. H. Cho, and G. I. Gellene. 2000. Refractive index mysteries of water. *J. Phys. Chem. B.* 104:7179–7182.
62. Petrenko, V. F., and R. W. Whitworth. 1999. Physics of Ice. Oxford University Press, New York.
63. Sicheri, F., and D. S. Yang. 1995. Ice-binding structure and mechanism of an antifreeze protein from winter flounder. *Nature.* 375: 427–431.
64. Strausky, H., J. R. Krenn, A. Leitner, and F. R. Aussenegg. 1996. Thickness determination of a water film on dye-doped ice by fluorescence spectroscopy. *Appl. Opt.* 35:198–200.
65. Berg, H. C. 1993. Random Walks in Biology. Princeton University Press, Princeton, NJ.
66. Kubitscheck, U., O. Kuckmann, T. Kues, and R. Peters. 2000. Imaging and tracking of single GFP molecules in solution. *Biophys. J.* 78:2170–2179.